A Novel Antimony Sulfide Templated by Dimethylammonium: Its Synthesis and Structural Characterization Using Synchrotron/Imaging Plate Data

Kemin Tan,[†] Younghee Ko,[†] John B. Parise,*[,†,‡] Jae-Hyun Park,[‡] and Alex Darovsky[§]

CHiPR & Department of Earth and Space Sciences, State University of New York, Stony Brook, New York 11794; Department of Chemistry, State University of New York, Stony Brook, New York 11794; SUNY X3A Beamline, National Synchrotron Light Source, Brookhaven National Laboratory, Upton, New York 11973

Received April 17, 1996. Revised Manuscript Received June 26, 1996[⊗]

Hydrothermal synthesis at 200 °C produced a new open antimony sulfide framework, $[C_2H_8N]_2[Sb_8S_{12}(S_2)]$, designated DMA-SbS-SB8. The structure (*Cmca*, $a = 9.9704(7)$, $b = 11.652(2)$, and $c = 25.979(3)$ Å), determined from data collected on a small single crystal ($20 \times 30 \times 40$ μm in size) utilizing the synchrotron/imaging plate system installed at the X3A1 beamline of the NSLS, consists of $[Sb_8S_{12}(S_2)]^{2-}$ double chains formed from $Sb_4S_7^{2-}$ single chains joined through S−S bridges. The double chains contain 18-membered Sb_8S_{10} rings and are interlocked to form sheets perpendicular to the *b* axis. Dimethylammonium ions, assumed to be protonated to charge balance the anionic $[Sb_8S_{12}(S_2)]^{2-}$ framework, reside within 18-membered rings. The structural building units of the new open framework are similar to those described previously in other members of the antimony sulfide system. Experiments carried out at different temperatures and reaction times show that DMA-SbS-SB8 is formed from a distinct poorly crystallized phase (designated DMA-SbS-SB8′), which is the dominant phase at 100 °C.

Introduction

By applying well-known hydrothermal techniques used for the production of oxide molecular sieves, a variety of novel open metal chalcogenide frameworks have been synthesized over the past decade.[1−31] These structures are often characterized by common secondary building units such as ($Sb_3S_6^{3-}$),[9−11,32] ($Sn_3S_7^{2-}$),[19−24] and ($Ge_4S_{10}^{4-}$)[15,25−31] and contain large pores which are often occupied by organic molecules added to the starting materials and believed to act as templates. The manner in which these units polymerize is dependent upon the types of the organic templates and can also be influenced by the addition of transition metals.[15,26,27,29−31] Recently, the number of sulfide frameworks synthesized according to these strategies and structurally characterized has increased steadily. Some distinctive structural relationships have emerged from this database, which may be useful to understand-

[†] CHiPR, Center for High Pressure Research: NSF Funded Science and Technology Center.
[‡] Department of Chemistry.
[§] Brookhaven National Laboratory
[⊗] Abstract published in *Advance ACS Abstracts,* September 1, 1996.

(1) Krebs, B. *Angew. Chem., Int. Ed. Engl.* **1983**, *22*, 113−134.
(2) Graf, H. G.; Schäfer, H. *Z. Naturforsch.* **1972**, *27b*, 735−739.
(3) Volk, K.; Schäfer, H. *Z. Naturforsch.* **1979**, *34b*, 1637−1640.
(4) Dittmar, V. G.; Schäfer, H. *Z. Anorg. Allg. Chem.* **1978**, *441*, 93−97.
(5) Eisenmann, B.; Schäfer, H. *Z. Naturforsch.* **1979**, *34b*, 383−385.
(6) Volk, K.; Schäfer, H. *Z. Naturforsch.* **1979**, *34b*, 172−175.
(7) Sheldrick, W. S.; Haüsler, H. J. *Z. Anorg. Allg. Chem.* **1988**, *557*, 105−111.
(8) Sheldrick, W. S.; Haüsler, H. J. *Z. Anorg. Allg. Chem.* **1988**, *561*, 149−156.
(9) Parise, J. B. *Science* **1991**, *251*, 293−294.
(10) Parise, J. B.; Ko, Y. *Chem. Mater.* **1992**, *4*, 1446−1450.
(11) Tan, K.; Ko, Y.; Parise, J. B. *Acta Crystallogr.* **1994**, *C50*, 1439−1442.
(12) Wang, X.; Liebau, F. *J. Solid State Chem.* **1994**, 385−389.
(13) Wang, X. *Eur. J. Solid State Inorg. Chem.* **1995**, *32*, 303−312.
(14) Ko, Y.; Tan, K.; Parise, J. B.; Darovsky, A. *Chem. Mater.* **1996**, *8*, 493−496.
(15) Bedard, R. L.; Wilson, S. T.; Vail, L. D.; Bennett, J. M.; Flanigen, E. M. In Zeolites: Facts, Figures, Future. Proceedings of the 8th International Zeolite Conference; Jacobs, P. A., Santen, R. A. v., Eds.; Elsevier: Amsterdam, 1989, 375−387.
(16) Bedard, R. L.; Vail, L. D.; Wilson, S. T.; Flanigen, E. M. U.S. Patent 4,880,761, 1989.
(17) Bedard, R. L.; Vail, L. D.; Wilson, S. T.; Flanigen, E. M. U.S. Patent 4,933,068, 1990.
(18) Parise, J. B.; Ko, Y.; Rijssenbeek, J.; Nellis, D. M.; Tan, K.; Koch, S. *J. Chem Soc., Chem. Commun.* **1994**, 527.
(19) Parise, J. B.; Ko, Y. *Chem. Mater.* **1994**, 6, 718−720.
(20) Parise, J. B.; Ko, Y.; Tan, K.; Nellis, D. M.; Koch, S. *J. Solid State Chem.* **1995**, *117*, 219−228.
(21) Ko, Y.; Tan, K.; Nellis, D. M.; Koch, S.; Parise, J. B. *J. Solid State Chem.* **1995**, *114*, 506−511.
(22) Tan, K.; Ko, Y.; Parise, J. B. *Acta Crystallogr.* **1995**, *C51*, 398−401.
(23) Jiang, T.; Ozin, G. A.; Bedard, R. L. *Adv. Mater.* **1994**, *6*, 860−865.
(24) Ahari, H.; Ozin, G. A.; Bedard, R. L.; Petrov, S.; Young, D. *Adv. Mater.* **1995**, *6*, 370−374.
(25) Pivan, J. Y.; Achak, O.; Loüer, M.; Loüer, D. *Chem. Mater.* **1994**, *6*, 827−830.
(26) Yaghi, O. M.; Sun, Z.; Richardson, D. A.; Groy, T. L. *J. Am. Chem. Soc.* **1994**, *116*, 807−808.
(27) Tan, K.; Darovsky, A.; Parise, J. B. *J. Am. Chem. Soc.* **1995**, *117*, 7039−7040.
(28) Nellis, D. M.; Ko, Y.; Tan, K.; Koch, S.; Parise, J. B. *J. Chem Soc., Chem. Commun.* **1995**, 541−542.
(29) Tan, K.; Ko, Y.; Parise, J. B.; Darovsky, A. *Chem. Mater.* **1996**, *8*, 448−453.
(30) Achak, O.; Pivan, J. Y.; Maunaye, M.; Loüer, M.; Loüer, D. *J. Solid State Chem.* **1996**, *121*, 473−478.
(31) Parise, J. B.; Tan, K. *J. Chem. Soc., Chem. Commun.* submitted.
(32) MaCarthy, T. J.; Kanatzidis, M. G. *Inorg. Chem.* **1994**, *33*, 1205−1211.

S0897-4756(96)00239-6 CCC: $12.00

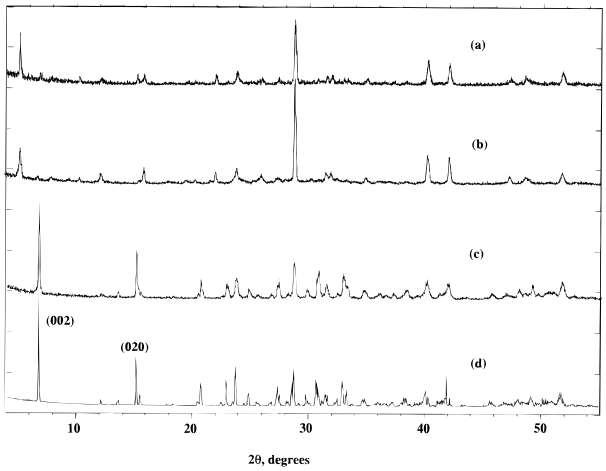

Figure 1. X-ray powder diffraction patterns of (a) the mixture of needle (DMA-SbS-SB8′) and plate-shaped crystals (DMA-SbS-SB8), (b) pure DMA-SbS-SB8′, and (c) pure DMA-SBS-SB8. The experiment was performed on a Scintag diffractometer with Cu Kα (λ = 1.5406 Å) radiation. (d) Calculated X-ray powder diffraction pattern[40] of DMA-SbS-SB8 based on the structure model obtained from the single-crystal X-ray diffraction study (Tables 1 and 2).

ing the structural systematics of these chalcogenide compounds and directing future syntheses.

In this paper, we report the synthesis of a novel antimony sulfide framework $[C_2H_8N]_2[Sb_8S_{12}(S_2)]$ (designated DMA-SbS-SB8) and its structural characterization with data collected by utilizing the synchrotron/imaging plate system.[14,27,29,31] We also analyze its structural relationships with other known open antimony sulfide frameworks and its evolution from a poorly crystallized and structurally distinct phase (designated DMA-SbS-SB8′).

Experimental Section

Synthesis and Characterization. Dimethylamine was used in an attempt to direct the crystallization of an open-framework antimony sulfide.[10] To a mixture of antimony metal (0.24 g, Alfa) and elemental sulfur (0.10 g, Alfa), a 40 wt % dimethylamine (DMA) solution (1.5 g, Aldrich) was added to form a slurry. This was heated at 200 °C under thiosulfate bearing hydrothermal conditions in a Pyrex-lined bomb.[14] After 1 day the products were washed with water and ethanol and dried in air. They were a mixture of needle- and plate-shaped crystals. The needles were typically 0.01 × 0.01 × 0.20 mm in dimension with some up to 0.5 mm in length. The plate-shaped crystals were usually less than 0.05 mm on edge and typically 0.02 × 0.04 × 0.04 mm in dimension. The two types of crystals had a similar dark red color. The powder diffraction pattern of the mixture is shown in Figure 1a. Three plate-shaped crystals from the batch were chosen for examination with the single-crystal synchrotron/imaging plate techniques described in detail below. However, because the X-ray reflections from these crystals were diffuse, they were unsuitable for further study.

Another batch of the same reagents was heated for 3 days at 200 °C. Only plate-shaped crystals were present. They were washed and the yield was calculated to be 90% based on antimony metal. Crystals from this batch were used for structural analysis, which confirmed they were of a new phase, designated as DMA-SbS-SB8.[10] The powder diffraction pattern of the phase (Figure 1c) is consistent with that calculated from the structural model (Tables 1, 2 and Figure 1d). Comparison between parts a and c of Figure 1 suggested that the needle crystals from the first batch, referred to as DMA-SbS-SB8′, were a distinct material.

To isolate DMA-SbS-SB8′, other experiments were carried out with shorter reaction times or at 100 °C. The products were always a mixture of two phases when heating at 200 °C for less than 1 day. However, at 100 °C only needle-shaped crystals of DMA-SbS-SB8′ were produced, even after 7 days. The needle shaped crystals examined at the synchrotron were found to be poorly crystallized. The powder ground from them was slightly brownish, and the X-ray powder diffraction pattern is shown in Figure 1b.

Quantitative electron-probe microanalysis was carried out on samples of DMA-SbS-SB8 and DMA-SbS-SB8′ using a Cameca Camebax instrument. The accelerating voltage was set to 20 kV, and the beam current to 10 nA. A rastered beam of 20 μm was used in order to reduce beam damage. The measured weight percentages of Sb and S in DMA-SbS-SB8 were 65.06 ± 0.48 and 28.82 ± 0.55, respectively, leaving a residual of 6.12% to undetectable elements such as N, C, and H. These results are consistent with the composition derived from the crystal structure (Table 1). For DMA-SbS-SB8′, a trial compositional analysis was made with a 5 μm rastered beam and higher magnification. The electron radiation damage was so serious that sample crystals decomposed quickly. An analysis by plasma emission spectroscopy (for Sb) and high-temperature combustion (for S and N) was done for DMA-SbS-SB8′, resulting in a molar ratio of Sb:S:N = 4:12.24:1.20, which is sulfur rich with respect to DMA-SbS-SB8 (Table 1).

The IR spectra of DMA-SbS-SB8 and DMA-SbS-SB8′ were recorded from 4000 to 400 cm^{-1} on a Perkin-Elmer 1600 Series FT-IR spectrophotometer using KBr pellets. The distribution of absorption peaks in both spectra were very similar. All peaks were only 5−20% above background, and this might be due to the low concentration of organic material in both compounds. Resolvable peaks were located at 3062.6 (wide), 1564.9, 1442.3, 1397.6, 1371.5, 1007.8, 879.7, and 809.1 cm^{-1}. All except the peak at 809.1 cm^{-1} match the pattern expected for dimethylamine;[33] this confirms the existence of this molecule in both phases.

Synchrotron/Imaging Plate Data Collection and Processing. A crystal of DMA-SBS-SB8 was selected and mounted on a glass fiber 20 μm in diameter. X-ray diffraction data were collected at the beamline X3A1 of the National Synchrotron Light Sources (NSLS) at the Brookhaven National Laboratory. A scintillation detector was used to center 22 reflections from which an orientation matrix and cell parameters were determined (Table 1). An imaging plate (IP) cassette was then loaded on the 2θ arm of the Huber diffractometer in place of the scintillation detector. The first set of rotation photographic data was collected with no 2θ-arm offset. For each exposure the crystal rotated 8° with an overlap of 2° between successive exposures. Data were collected from 30 IPs within 4 h; experimental details are summarized in Table 1.

From the orientation matrix and the distribution of reflection spots on the IPs, it was noticed that the rotation axis was close to the *b* axis of the crystal's unit cell. This was later confirmed by studying the distribution of recorded reflections in reciprocal space. This orientation generated a blind zone around the *b** axis and in order to collect as many unique reflections as possible, another data set was collected with the goniometer offset 36° from its original position and the 2θ arm at 30°. The alternation of crystal orientation can also be achieved by using an elbow device.[34] To avoid overlapping of reflection spots on one IP while collecting as many reflections on each IP as possible for intensity scaling between plates, the ϕ oscillation range for each exposure was varied from 6° to 10°. From Figure 2 it is clear that the second data set covers a wider range of $(\sin\theta)/\lambda$.

Each image was processed to obtain the refined crystal-to-plate distance and the IP tilt angles.[35] Examination of the reflection extinction conditions suggested a C centered lattice.

(33) *The Aldrich Library of Infrared Spectra*, 3rd ed.; Pouchert, C. J., Ed.; Aldrich Chemical Company Inc.: Milwaukee, 1981.
(34) Pressprich, M. R.; Fransen, B.-J.; Darovsky, A.; Coppens, P. *J. Appl. Cryst.* **1995**, *28*, 650.
(35) Bolotovsky, R. The IPMS program, Chemistry Department, State University of New York, Buffalo, New York.

Table 1. Selected Crystallographic Data for the Synchrotron/Imaging Plate Experiment for DMA-SbS-SB8

Crystal Data	
chemical formula	$[C_2H_8N]_2[Sb_8S_{12}(S_2)]$
chemical formula weight	1537.8
crystal system	orthorhombic
space group	*Cmca*
unit cell	$a = 9.9704(7)$ Å, $b = 11.652(2)$ Å, $c = 25.979(3)$ Å
volume of unit cell	3018.1(7) Å^3
formula per unit cell, Z	4
density calcd from formula and cell	3.345 g cm^{-3}
radiation type and wavelength	synchrotron, $\lambda = 0.642(1)$ Å
no. of reflns for cell measurement and 2θ range	22 reflections, $16.1° < 2\theta < 36.6°$
measurement temp	293 K
crystal shape, color and size	plate, dark red, 0.02 × 0.03 × 0.04 mm
Data Collection	
data-collection method	imaging plate
imaging plate	Fuji imaging plate, medical, high resolution, HR-V, 20 × 25 cm
scanner	Fuji, Bio-imaging analyzer, BAS2000
2θ offset of image plate cassette	1st set 0°; 2nd set 30°
crystal to imaging plate distance	1st set 142 mm; 2nd set 160 mm
no. of images exposed	1st set 30; 2nd set 29
oscillation angle	6−10°
overlap angle	1°
ϕ range	180°
gradation and latitude	1024, 4
resolution	100 μm
sensitivity	1st set 10000; 2nd set 6000
no. of reflns integrated ($I > 1.0\sigma(I)$)	8968
no. of unique reflections	2027
merge R (based on I)	0.035
minimum, maximum value of $(\sin\theta)/\lambda$	0.101, 0.833
absorption coefficient	37.96 cm^{-1}
absorption correction	none
Refinement	
refinement on	F^2
final $R(F)$, $wR(F^2)$ for all integrated reflections	0.0409, 0.1362
goodness-of-fit for all integrated reflections	1.226
no. of parameters refined	76
no. of reflns used	2027
maximum shift/esd	0.008
residual electron densities	$\Delta\rho_{min} = -1.51$ eÅ^{-3}, $\Delta\rho_{max} = 1.48$ e Å^{-3}

Table 2. Fractional Atomic Coordinates and Equivalent Isotropic Displacement Parameters ($\times 10^3$ Å^2) for DMA-SbS-SB8

atom	x	y	z	U
Sb1	0.30365(5)	1.09976(4)	0.31994(2)	21.62(14)
Sb2	0.0000	0.96559(6)	0.38871(2)	23.3(2)
Sb3	0.5000	0.86321(6)	0.25591(3)	25.1(2)
S1	0.5000	1.1367(3)	0.37584(10)	26.5(5)
S2	0.1809(2)	1.1013(2)	0.40258(7)	28.6(4)
S3	0.5000	1.0569(2)	0.22556(9)	22.8(5)
S4	0.0000	0.9191(3)	0.48285(10)	35.1(7)
S5	0.3168(2)	0.8877(2)	0.31972(7)	27.4(4)
N1	0.5000	0.8374(12)	0.4333(5)	48(3)
H1a[a]	0.5000	0.7538(12)	0.4244(5)	213(119)
H1b[a]	0.5000	0.8814(12)	0.4002(5)	213(119)
C1	0.3756(14)	0.8641(11)	0.4616(4)	59(3)
H2a[b]	0.3002(23)	0.8167(56)	0.4475(23)	92(29)
H2b[b]	0.3538(50)	0.9473(19)	0.4575(28)	92(29)
H2c[b]	0.3882(32)	0.8461(72)	0.4989(7)	92(29)

[a] The coordinates of the two hydrogen atoms attached to N1 were calculated and then refined with a "riding model".[40] [b] The coordinates of the three hydrogen atoms attached to C1 were calculated and then refined with a "rotating model".[40]

From two data sets a total of 8968 fully recorded allowed reflections with $I > 1.0\ \sigma(I)$ were integrated using the "seed-skewness" method.[36] Those close to the oscillation axis were rejected due to the distorted spot shapes on the IP. Reflections close to IP margins or oscillation boundaries were also ignored because of the possibility of their being partially recorded and nonlinear exposure during the acceleration and deceleration of the rotation motor.

Structure Determination and Refinement. Inspection of systematically absent reflections suggested extinction symbol C--2_1. The data were merged in point group 222, and a structure model was obtained in space group $C222_1$ by using the direct methods in SHELXS86.[37] Subsequent refinement, difference Fourier synthesis and analysis of possible missing symmetry was carried out using a package of programs written and maintained by Calabrese.[38] The results strongly suggested the presence of an inversion operator, through which positions of crystallographically unique atoms were related within 4σ to others in the atom list. We concluded that *Cmca* is the correct space group, although six weak reflections violated this symmetry. These reflections were some 300 times weaker than the strongest observed and were attributed to effects not related to the choice of space group, such as multiple reflection.[39] A similar phenomenon was observed and discussed in our other synchrotron/imaging plate studies.[29] The raw integrated reflections were then merged in point group *mmm* and the final refinements in *Cmca* against F^2 were carried out using SHELXL93.[40] The hydrogen atoms on either nitrogen or carbon atoms of the template molecules were not located in Fourier difference maps. Their ideal positions were calculated and refined using the "riding" or "rotating" models in SHELXL93.[40] Final atomic parameters and selected interatomic distances and angles are given in Tables 2 and 3.

(36) Bolotovsky, R.; White, M. A.; Darovsky, A.; Coppens, P. *J. Appl. Cryst.* **1994**, *28*, 86−95.

(37) Sheldrick, G. M. SHELXS86, Program for the Solution of Crystal Structures; University of Göttinggen, Germany, 1985.

(38) Calabrese, J. C. The Z package of programs, EI DuPont, Wilmington, DE, 1988.

(39) Renninger, M. *Z. Phys.* **1937**, *106*, 141.

(40) Sheldrick, G. M. SHELXL93, Program for the Refinement of Crystal Structures; University of Göttinggen, Germany, 1993.

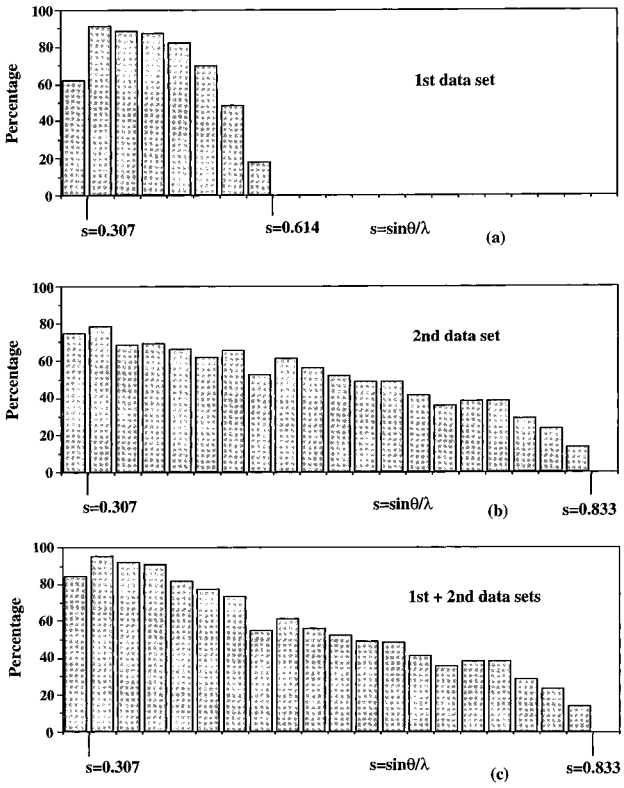

Figure 2. Percentage of unique reflections measured with $I > 1.0\sigma(I)$ in equal-volume shells of $s = (\sin\theta)/\lambda$ for (a) the first set of data, (b) the second set of data, and (c) the combination of two sets of data.

Table 3. Selected Interatomic Distances (Å) and Angles (°) for DMA-SbS-SB8

Sb1−S2	2.471(2)	S2−Sb1−S5	92.04(7)
Sb1−S5	2.474(2)	S2−Sb1−S1	83.15(7)
Sb1−S1	2.475(2)	S5−Sb1−S1	97.66(9)
Sb2−S2	2.426(2)	S2[a]−Sb2−S2	96.07(11)
Sb2−S2[a]	2.426(2)	S2[a]−Sb2−S4	89.77(7)
Sb2−S4	2.505(3)	S2−Sb2−S4	89.77(7)
Sb3−S3	2.390(3)	S3−Sb3−S5[b]	96.41(7)
Sb3−S5	2.483(2)	S3−Sb3−S5	96.41(7)
Sb3−S5[b]	2.483(2)	S5[b]−Sb3−S5	94.72(10)
S4−S4[c]	2.085(7)	Sb1−S1−Sb1[b]	104.54(9)
N1−C1	1.475(14)	Sb2−S2−Sb1	103.56(7)
		S4[c]−S4−Sb2	102.8(2)
Sb2···S3[d,i]	3.147(2)	Sb1−S5−Sb3	98.94(7)
Sb1···S3[i]	3.173(2)	C1[b]−N1−C1	114.5(13)
Sb1···S3[d,i]	3.287(3)		
Sb1···S5[e,i]	3.560(3)		
Sb2···S4[f,i]	3.590(3)		
Sb3···S3[g,i]	3.597(3)		
S2···N1[h,j]	3.380(8)		

[a] −*h*Symmetry operation codes: (a) $-x, y, z$; (b) $1 - x, y, z$; (c) $-1 - x, 2 - y, 1 - z$; (d) $-^1/_2 + x, y, ^1/_2 - z$; (e) $^1/_2 - x, ^1/_2 + y, z$; (f) $x, 2 - y, 1 - z$; (g) $x, -^1/_2 + y, ^1/_2 - z$; (h) $-^1/_2 + x, ^1/_2 + y, z$.[i] The Sb-S interactions with interatomic distances larger than 3.140 Å are not considered in defining primary building units or SbS polyhedra. [j] The shortest distance between the nitrogen atom of DMA and the sulfur atom from framework, implying a possible hydrogen bonding between the template and the framework.

Results and Discussion

Structural Characteristics of DMA-SbS-SB8. The structure contains three unique Sb(III) atoms. Each is coordinated to three S atoms with bond lengths ranging from 2.390(3) to 2.505(3) Å and S−Sb−S angles from 83.15° to 94.61° (Table 3), forming an SbS_3^{3-} trigonal pyramidal primary building unit (Figure 3). The formal bond valence of each Sb−S bond is calculated to be greater than 0.88 v.u. and their sums for one antimony are from 2.83 to 3.02 v.u.[41] Each antimony has one-to-three additional sulfur near neighbors at distances ranging from 3.147(2) to 3.597(3) Å (Table 3) with calculated formal bond valence less than 0.22 v.u.[41] These weak interatomic interactions are not considered in the definition of the primary building units and SbS polyhedra but represent interactions between higher level structural building units discussed below.

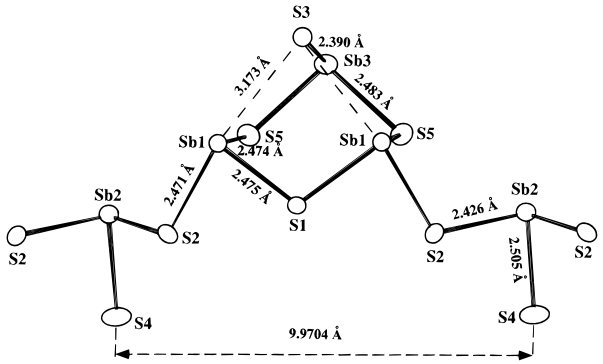

Figure 3. ORTEP[43] drawing of a semicube secondary building unit and its connection to individual SbS_3^{3-} pyramids. Semicubes and individual pyramids are connected alternatively along [100], forming a single chain of composition $Sb_4S_7^{2-}$. The Sb−S interactions with interatomic distances larger than 3.140 Å are shown (Table 3). Ellipsoids are drawn at 50% probability.

Three SbS_3^{3-} pyramids form an $Sb_3S_6^{3-}$ semicube (Figure 3), which is a common secondary building unit found in antimony sulfides.[9−11,14,32] The alternative connection of semicubes and individual pyramids forms $Sb_4S_7^{2-}$ single chains, which are paired to make $Sb_8S_{12}(S_2)^{2-}$ double chains through S−S bridges (Figure 4a). The connection generates an Sb_8S_{10} 18-membered ring, containing two dimethylamine (DMA) molecules. The nitrogen atom from each DMA is positioned at the corner of an $Sb_3S_6^{3-}$ semicube to complete a distorted cube (Figure 4) with its two $N-CH_3$ bonds pointing away from the cube. Since the double chain is anionic, the DMA molecules are assumed to be protonated for charge balance. This leads to a chemical formula for DMA-SbS-SB8, $[C_2H_8N]_2[Sb_8S_{12}(S_2)]$.

The $Sb_8S_{12}(S_2)^{2-}$ double chains lie in the (010) plane of the structure and interlock in a zipperlike arrangement (Figure 4a) allowing interactions to form sheets. These are typified by Sb2···S3 (3.147(2) Å) and Sb1···S3 (3.173(3) Å) interatomic distances (Table 3). The sheets are then stacked perpendicular to the *b* axis with intersheet interactions characterized by Sb1···S5 (3.560-(3) Å; Figure 4b and Table 3). The shortest distance between the dimethylammonium cation and its surrounding framework atoms is represented by the interatomic distance S(2)···N(1) [3.380(8) Å], implying possible H bonding between the template and the framework.

Structural Relationships between DMA-SbS-SB8 and Other Antimony Sulfides. The $Sb_4S_7^{2-}$ single chain, similar to those discussed above, also occurs as a common structural feature in the antimony sulfides templated by piperazinium (SBSpip or PIP-SbS-SB4,[10] Figure 5a), ethylenediammonium (SBSen or EN-SbS-SB5,[11] Figure 5b) and 1,3-propanediammonium[13]

(41) Slupecki, O.; Brown, I. D. *Acta Crystallogr.* **1982**, *B38*, 1078−1079.

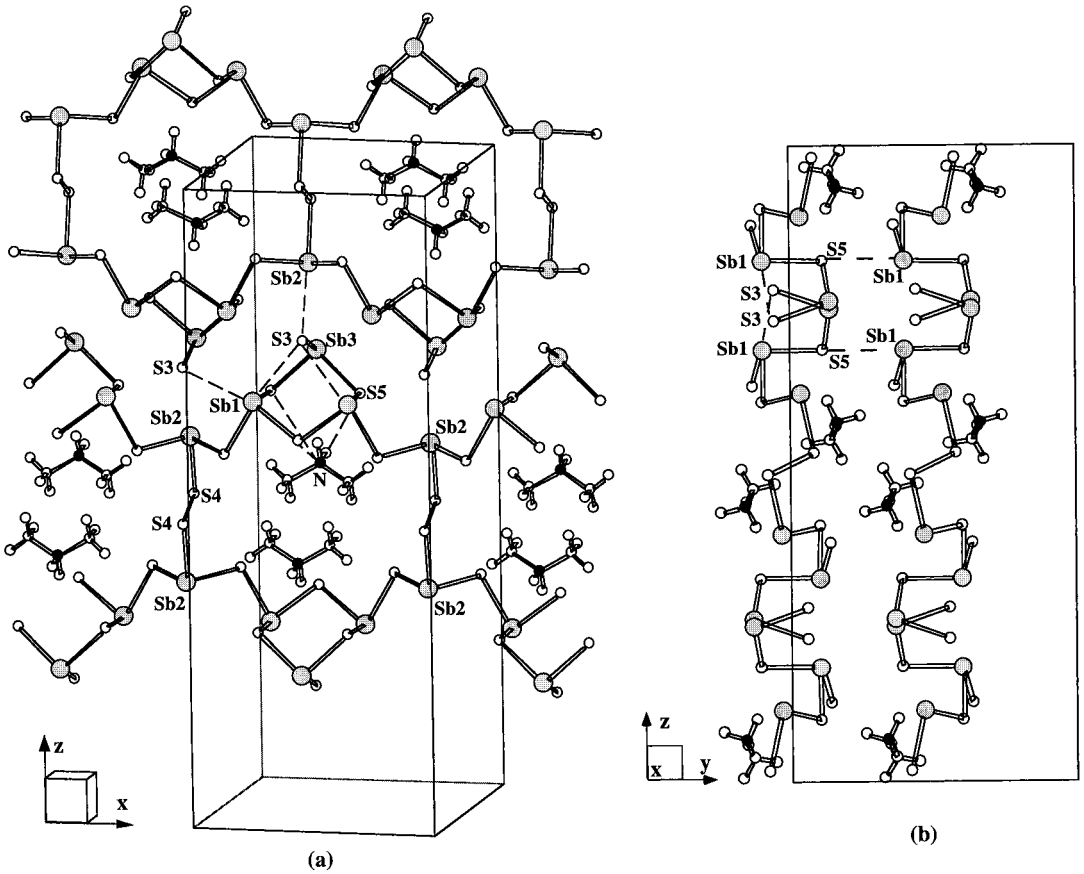

Figure 4. (a) Double chains interlocked in a "zipper" arrangement forming sheets (b) perpendicular to the *b* axis. Some of those interatomic distances (>3.140 Å for Sb···S and >3.300 Å for S···N) indicative of weaker interactions are shown as dotted lines. Two molecules of dimethylammonium, assumed to be protonated for charge balance, are arranged close to the 18-membered ring (Sb_8S_{10}) aperture in the sheet with the nitrogen atoms from them positioned close to the corner of the of $Sb_3S_6^{3-}$ semicubes to complete distorted cubes.

(Figure 5d). In PIP-SbS-SB4, single chains are paired through hydrogen bonding with piperaziniums, which separate them by 7.0 Å from each other.[10] The paired chains also interlock in a "zipper" arrangement resembling that found in DMA-SBS-SB8. In EN-SbS-SB5, the framework is very similar to that of DMA-SBS-SB8, except that single chains are connected through a single sulfur atom rather than a S_2 unit (Figure 5b,c). The structure templated by 1,3-propanediammonium[13] (Figure 5d) also consists of chains if Sb−S interactions with interatomic distances larger than 3.020 Å are not considered in defining SbS polyhedra.[13] In this case, the chains are connected through two SbS_3^{3-} pyramids (Figure 5d). The size differences of the apertures generated by the connection of single chains may be attributed to the size, charge, and shape of the templates. For example, the opening of the Sb_8S_8 16-membered ring (free dimension ≈1.2 × 6.3 Å) found in EN-SbS-SB5 is not big enough to enclose two protonated dimethylamine molecules, which are approximately 2.6 × 4.7 Å/molecule. Instead, an Sb_8S_{10} 18-membered ring (free dimension ≈2.8 × 6.3 Å) is formed in DMA-SbS-SB8 to create a bigger aperture for two dimethylammonium molecules. The free dimensions are estimated assuming 3.70 Å as the van der Waals radius of the sulfurs lining the inner peripheries of the quasi-rectangular openings in these structures.

Although not every antimony sulfide has such building units, the persistence of the $Sb_4S_7^{2-}$ single chain in the compounds discussed above suggests it is one of the important structural building blocks in the synthesis of open antimony sulfides. Structures based on this building unit have their unique topologies, which can be systematized. Single chains consisting of alternating SbS_3^{3-} pyramids and $Sb_3S_6^{3-}$ semicubes give rise to a repeat distance of about 10 Å (Figure 3). The chains are likely to be paired or to be bridged, forming quasi-rectangular openings with free dimension about 6.3*L* Å, where *L* is determined by the way in which a pair of chains is connected. For example, it is 1.2 Å for the single sulfur bridge in EN-SbS-SB5[11] and 2.8 Å for the S−S bridge in DMA-SBS-SB8 (Tables 1 and 2 and Figure 5c). The paired single chains or double chains in most cases are like rigid slabs with zipperlike structural components (semicubes) on both sides. They interlock to form parallel stacked sheets. The interactions between interlocked double chains or between neighboring sheets are usually represented by some weak Sb···S interactions with interatomic distances about 3.1−3.5 Å (Table 3 and refs 10, 11, and 13).

This way of generating open antimony sulfide frameworks can create, in addition to the known structures, a range of as-yet-unsynthesized structures. Since the variation of the frameworks in this system is mainly caused by the different ways in which single chains are bridged, modification of the reaction pathway may lead to different structural motifs.

DMA-SbS-SB8 and DMA-SbS-SB8′. Some of the features of DMA-SbS-SB8' can be deduced, though its structure is unknown. The similarities in the IR absorption spectra of DMA-SbS-SB8 and DMA-SbS-8′ suggest that both phases contain the same templates.

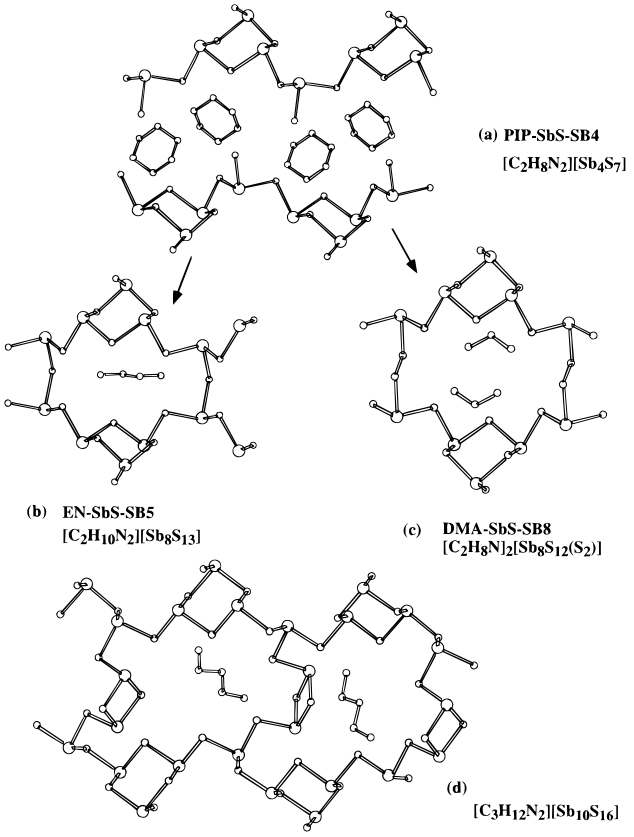

Figure 5. Structural relationship between some antimony sulfide frameworks templated by (a) piperazinium (SbSpip or PIP-SbS-SB4),[10] (b) enthylenediamomnium (SbSen or EN-SbS-SB5),[11] (c) dimethylammonium (DMA-SbS-SB8), and (d) 1,3-propanediammonium.[13]

The common reflections, at $2\theta = 23.80°$, 28.71°, 40.12°, and 41.97° for example (Figure 1b,c) in their X-ray powder diffraction patterns, suggest that both phases share common structural features. One reasonable assumption is that DMA-SbS-SB8′ contains similar paired single chains as DMA-SbS-SB8 and the other compounds discussed above. From the systematics of these frameworks, the difference between DMA-SbS-SB8′ and DMA-SbS-SB8 likely arises from the way in which single chains are connected. In the X-ray powder diffraction patterns (Figure 1b,c) the most obvious distinction between these two phases is the position of their first peaks. For DMA-SbS-SB8 (Figure 1c), the (002) reflection is located at 6.799° and represents the repeat of the double chains ($d = 12.990$ Å) along the c axis (Figure 4). For DMA-SbS-SB8′, the first peak is located at 5.152° (Figure 1b) corresponding a d space of 17.229 Å. Since the repeat distance of the single chain is about 10 Å and the period of stacked sheets less than 10 Å, one possible source of the reflection is the repeat of double chains within sheets.

Considering that DMA-SbS-SB8′ is sulfur rich compared to DMA-SbS-SB8, single chains in DMA-SbS-SB8′ may be connected through $(S_n)^{2-}$ ($n > 2$) units rather than the $(S_2)^{2-}$ units found in DMA-SbS-SB8. The $(S_n)^{2-}$ ($n > 2$) connection has been observed in the structure of $CsSbS_6$, in which $(S_5)^{2-}$ units are found.[32] If the first peak in the powder diffraction pattern of DMA-SbS-SB8′ represents the repeat of double chains, the $(S_n)^{2-}$ unit could be estimated to be $(S_6)^{2-}$ since the S−S bond length is about 2.05 Å and the S−S−S bond angle is about 106°.[42]

Experimentally, DMA-SbS-SB8′ can nucleate over a wider temperature range and transform to DMA-SbS-SB8 at 200 °C only under hydrothermal conditions. Following the transformation, the crystallinity of the DMA-SbS-SB8 structure increases with time. This accounts for the high quality of the single crystals of the phase after heating at 200 °C for 3 days. The mechanism of the transformation is unclear and requires a detailed structure for DMA-SbS-8′. This, and a real-time study of the processes involved in the transformation between these two phases, are in progress. Results from these experiments will aid future synthetic efforts and structure design.

Acknowledgment. We thank the National Science Foundation (DMR 94-13003) for financial support. Research carried out in part at the National Synchrotron Light Source at Brookhaven National Laboratory which is supported by the U.S. Department of Energy, Division of Materials Sciences and Division of Chemical Sciences. The SUNY X3 beamline at the NSLS is supported by the Division of Basic Energy Sciences of the U.S. Department of Energy (DE-FG02-86ER45231).

Supporting Information Available: Anisotropic displacement factors (1 page); structure factors (17 pages). Ordering information is given on any current masthead page.

CM9602398

(42) Cotton, F. A.; Wilkinson, G. *Advanced Inorganic Chemistry*; John Wiley & Sons: New York, 1988.
(43) Johnson, C. K. ORTEP, ORNL Report 5138, Oak Ridge National Laboratory, Oak Ridge,TN, 1976.